ACS APPLIED MATERIALS & INTERFACES

Article

Binary Nanoparticle-graphene Hybrid Structure-based Highly Sensitive Biosensing Platform for Norovirus-like Particle Detection

Jaewook Lee, Kenshin Takemura, Chika Nozaki Kato, Tetsuro Suzuki, and Enoch Y. Park

ACS Appl. Mater. Interfaces, **Just Accepted Manuscript** • DOI: 10.1021/acsami.7b07012 • Publication Date (Web): 28 Jul 2017

Just Accepted

ACS Publications

ACS Applied Materials & Interfaces is published by the American Chemical Society.
1155 Sixteenth Street N.W., Washington, DC 20036

Binary Nanoparticle-graphene Hybrid Structure-based Highly Sensitive Biosensing Platform for Norovirus-like Particle Detection

Jaewook Lee,[†] Kenshin Takemura,[‡] Chika Nozaki Kato,[¶] Tetsuro Suzuki,[§] Enoch Y. Park[†,‡,*]

[†]Research Institute of Green Science and Technology, Shizuoka University 836 Ohya Suruga-ku, Shizuoka 422-8529, Japan

[‡] Graduate School of Integrated Science and Technology, [¶]Department of Chemistry, Shizuoka University 836 Ohya Suruga-ku, Shizuoka 422-8529, Japan

[§]Department of Infectious Diseases, Hamamatsu University School of Medicine, 1-20-1 Higashi-ku, Handa-yama, Hamamatsu 431-3192, Japan

ABSTRACT: Nanoparticle-decorated carbon nanotubes or graphenes have attracted attention because of their synergic properties such as enhanced electrical conductivity, magneto-optical effect and plasmon resonance energy transfer. These hybrid carbon nanomaterials are widely used in sensing platforms to monitor target biomolecules, gases, and chemicals. In this study, binary nanoparticles, specifically gold (Au)/magnetic nanoparticle (MNP)-decorated graphenes (GRPs), were applied in a virus-sensing platform. This hybrid material exhibited multiple functionalities, including magnetic, plasmonic and enhanced electrical properties. Au/MNP-GRPs were synthesized in 2 steps at room temperature under mild conditions and magnetically deposited on a Pt-interdigitated electrode (IDE) as electrical-sensing channels. After deposition onto the electrode, the surface of Au/MNP-GRPs was conjugated with norovirus antibody (Ab) to produce a norovirus-like particle (NoV-LP)-sensing platform. NoV-LPs were successfully detected by the hybrid nanomaterial-sensing platform, exhibiting high sensitivity and specificity in a concentration range from 0.01 pg to 1 ng. In this case, the limit of detection was calculated as 1.16 pg/ml. Thus, binary-nanoparticle-decorated graphene shows excellent potential as an electrical-sensing platform for biomolecules.

KEYWORDS: *Binary nanoparticle-decorated graphene, Au/MNP-decorated graphene, Norovirus-like particle, electrical biosensor, magnetically deposited sensing channel*

1. INTRODUCTION

Nanoparticle-decorated carbon nanomaterials have been widely used in various fields as sensors, energy devices, drug delivery systems (DDSs) and optical devices because of their interesting synergic properties, including enhanced electrical and mechanical properties, catalytic activity, magneto-optical (MO) effect, and plasmonic resonance energy transfer.[1-3] Among diverse applications, such hybrid nanomaterials have been applied in several optical- and electrical-sensing platforms to monitor gases, biomolecules, and chemicals.[4-8] More specifically, multi-functional hybrid-nanomaterial-based sensing systems have been used to develop accurate diagnostic systems and on-site sensing systems with a rapid response time and high sensitivity and selectivity.[9,10] Indeed, various infectious diseases require early detection and frequent monitoring to prevent spread, thus improving human well-being and public safety.[11-13] To this end, hybrid nanomaterials and, eventually, nanoparticle-decorated carbon nanomaterials have been widely applied as biosensors, and various approaches have been used, including electrochemical-based detection, optical-property-based sensing platforms, and quartz crystal microbalance (QCM) sensors.[14-17]

Norovirus is a highly infectious virus with a critical pathogenesis because infection can occur with 100 or fewer virus particles in the human body.[18] This disease can also cause physical problems such as intense vomiting and diarrhea. In particular, infants and elderly people with lowered resistance might become severely sick.[19] Moreover, norovirus has shown negative effects and is considered an economic and health service burden.[20] Although several immune-chromatography-based detection kits for norovirus have been introduced, concerns about their sensitivity remain.[21,22] In addition, these detection systems are time-consuming and have poor cost performance.[23,24] Because no robust replication system exists for norovirus cell culture,[25,26] norovirus-like particles (NoV-LPs) have been used as target biomaterials for norovirus-sensing studies.[10,27]

In this study, we achieved a highly sensitive and selective sensing system for norovirus, whereby a Au-NP/magnetic-NP-decorated graphene (Au/MNP-GRP) hybrid structure was applied in electrical-sensing channels to monitor the electrical signal differences of biomolecules. In this case, Au/MNP-GRPs were magnetically deposited onto a Pt-interdigitated electrode (Pt-IDE) and functionalized by binding GII types of norovirus-specific antibodies (Abs) on the Au/MNP-GRP surface; the change in electrical resistance was then measured. To demonstrate the virus detection system, NoV-LPs were applied as target biomolecules for our system. First, the sensitivity test was performed with NoV-LP concentrations ranging from 0.01 pg/ml to 1 ng/ml. Second, several biomolecules, such as influenza virus (H7N7) antigen and bovine serum albumin (BSA) were used in the specificity test; the system displayed high sensitivity against other biomolecules. Thus, this system exhibited excellent detection performance.

2. EXPERIMENTAL SECTION

2.1. Materials and Instruments

$HAuCl_4 \cdot 3H_2O$ (99.9%), gallic acid monohydrate (GA; 3,4,5-trihydroxy benzoic acid monohydrate), $FeCl_3$, $FeCl_2 \cdot 4H_2O$, L-cysteine, N-ethyl-N'-(dimethylaminopropyl) carbodiimide (EDC), N-hydroxysuccinimide (NHS), 25% NH_4OH solution and BSA were obtained from Sigma-Aldrich Co. LLC (Tokyo, Japan). Graphene flakes (AO-3) were purchased from Graphene Supermarket (Calverton, NY, USA). The planar Pt-interdigitated electrode (Pt-IDE) was purchased from DropSens, S.L. (Llanera, Spain). Mouse anti-flavivirus group antigen monoclonal antibody (Ab) was obtained from EMD Millipore Corporation (Billerica, MA, USA). Goat anti-rabbit IgG-HRP was obtained from Santa Cruz Biotechnology (Paso Robles, CA, USA). Tetramethylbenzidine (TMBZ) was purchased from Dojindo (Kumamoto, Japan).

The plasmonic property of the Au/MNP-GRPs was measured using UV/Vis spectroscopy (Infinite® F500, TECAN, Ltd., Männedorf, Switzerland). The functional groups of GRP and the Au/MNP-GRPs were analyzed by FT-IR spectroscopy (FT-IR 6300, JASCO, Tokyo, Japan). The X-ray diffraction (XRD) patterns of the Au/MNP-GRPs were characterized using a powder X-ray diffractometer (RINT ULTIMA, Rigaku, Corp., Tokyo, Japan) with Cu Kα radiation and a Ni filter. The patterns were collected from 2 θ = 20 to 100° at a scan rate of 0.01° per step and 10 s per point. The magnetic properties of the MNPs and the Au/MNP-GRPs were measured using a superconducting quantum interference device (SQUID, MPMS-XL7, Quantum Design, Inc., San Diego, CA, USA). The surface morphologies of GA-MNPs, graphene and the Au/MNP-GRPs were observed using a transmission electron microscope (TEM, JEM-1400, JEOL, Tokyo, Japan), a high-resolution transmission electron microscope (HR-TEM, JEM-2100F, JEOL, Tokyo, Japan), and a scanning electron microscope (SEM, JSM-6510LV, JEOL, Tokyo, Japan). The Ab conjugation with the Au/MNP-GRPs was confirmed by an enzyme-linked immunosorbent assay (ELISA) with a plate reader (Model 680, Bio-Rad, Hercules, CA, USA). The conductivity of the Au/MNP-GRPs was measured, and NoV-LP detection was performed with a potentiometer (VersaSTAT 4, AMETEK Inc., Berwyn, PA, USA).

2.2. Synthesis of Au/MNP-GRPs

First, as the reducing agent and magnetic nanoparticles, GA-MNPs were prepared using the co-precipitation process. In this process, $FeCl_3$ (1 mmol, 0.1622 g) and $FeCl_2 \cdot 4H_2O$ (0.5 mmol, 0.0994 g) were dissolved in deionized (DI) water (20 ml), and 0.6 ml of 25% NH_4OH solution was added to the mixture and stirred for 10 min to form magnetic Fe_3O_4 NPs. Subsequently, GA (1.5 mmol, 0.255 g) powder was poured into the black Fe_3O_4 NP solution and stirred at 90 °C for 30 min. Because of the binding between GA and Fe in the GA-MNP

structure, the solution color changed from black to deep violet. After stirring, GA-MNPs were purified, precipitated with excess acetone and separated using a magnet.

Au/MNP-GRPs were synthesized in 2 steps. First, 5 mg of graphene and 10 mg of $HAuCl_4 \cdot 3H_2O$ (25 mmol) were dispersed in 40 ml of DI water by ultrasonication for 30 min. Then, 1 ml of GA-MNP solution (1 mg/ml concentration in DI water) was added into the Au^{3+}-GRP mixture. After 3 h of vigorous stirring, the hybrid material was separated by centrifugation and magnetic force and dried in the oven at 60 °C.

2.3. Bioconjugation Between Functionalized Nanomaterials and Antibody

To conjugate the mouse anti-flavivirus group antigen monoclonal antibody, the surface of Au/MNP-GRPs was modified with cysteamine for amine functionalization. First, 1 ml of 0.03 M cysteamine was added into the Au/MNP-GRP solution (1 mg/ml concentration). After 30 min of stirring, the amine-functionalized Au/MNP-GRPs were separated using a magnet, centrifuged (7500 rpm, 10 min) and dried in an oven. Bioconjugation and the virus detection process were performed in a polydimethylsiloxane (PDMS) well, which was attached on the Pt IDE (see Figure S2). To demonstrate the bioconjugation with Norovirus Ab, 15 µl (30 µg) of Au/MNP-GRPs (2 mg/ml concentration) was magnetically deposited onto the Pt-IDE and dried at room temperature. Then, 20 µl of EDC (0.1 M) was dropped and gently shaken for 30 min. Subsequently, 20 µl of NHS (0.1 M) was dropped and gently shaken for 5 min. Finally, 3 µl of GII norovirus-specific Ab (NV14, 1 µg/µl) was dropped and agitated for 16 h at 7 °C, and the electrode was washed with DI water. After Ab conjugation, the electrical conductivity was measured to evaluate the electrical resistance value before (R_0) and after (R_{Ab}) the Ab conjugation.

2.4. Virus Detection by the Ab-Conjugated Au/MNP-GRP Deposited Electrode

The sensitivity and specificity of the Ab-conjugated Au/MNP-GRP-deposited electrode sensing platform were monitored using a potentiostat. In this case, the sensitivity and specificity were evaluated via the resistance difference as shown in Equation (1).

$$\frac{\Delta R}{R_0} = \frac{\{R_{(\mathrm{Ab+vlp})} - R_{\mathrm{Ab}}\}}{R_{\mathrm{Ab}}} \qquad (1)$$

where $R_{(\mathrm{Ab+vlp})}$ and R_{Ab} are the electrical resistance values of the virus-sensing electrode and Ab-conjugated electrode, respectively. The prepared NoV-LP was a round particle with a virus surface covered with a cup-like protein, and its size was 38 nm, similar to that of native norovirus. The sensitivity of this sensing platform was tested using various concentrations (from 0.01 pg/ml to 1 ng/ml) of the target NoV-LPs. The binding processes of NoV-LPs and Ab were monitored via the resistance change of the sensing channel (Au/MNP-GRP) on the Pt-IDE. The specificity test was performed using several biomolecules, and each response was detected by measuring the electrical conductivity change. In this case, influenza virus antigens and BSA were used as biomolecules as a negative control. The NoV-LP production process is described in the supporting information (SI).[28]

3. RESULTS AND DISCUSSION

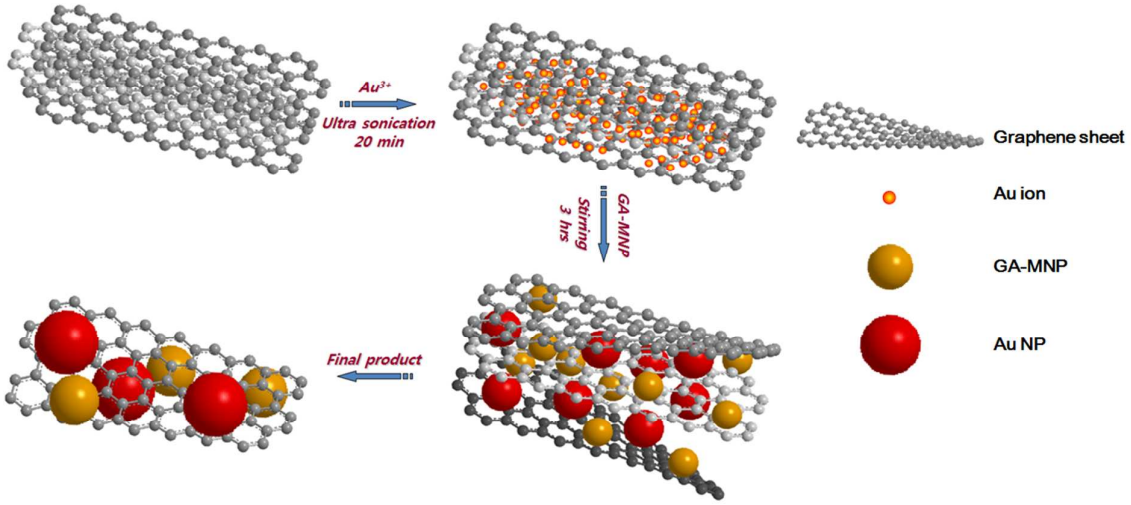

Figure 1. Schematic of Au/MNP-GRP preparation (not to scale).

Figure 1 depicts the synthetic scheme of Au/MNP-GRPs. This hybrid structure was prepared in 2 steps under mild conditions at room temperature. First, Au salt was dispersed with GRP in DI water via sonication. During this step, positive Au ions were placed and attached on the surface of GRP because the pi electrons on the GRP induced electrostatic interactions with the Au ions. Oxidizable GA-MNP was added to the mixture to reduce the Au ions to Au NPs on the GRP. Because of the anti-oxidant effect of GA, GA-MNP plays the role of the reducing agent for the Au NP synthetic process,[5,29] meaning that nucleation and island growth of Au NP occurs due to electrostatically attached Au ions on the GRP surface; as a result, Au NP could be physically attached to GRP. Simultaneously, the aromatic groups of the GA-MNP induced a pi-pi interaction with GRP. As a result, GA-MNPs can be decorated on the surface of GRP with Au NPs.[3]

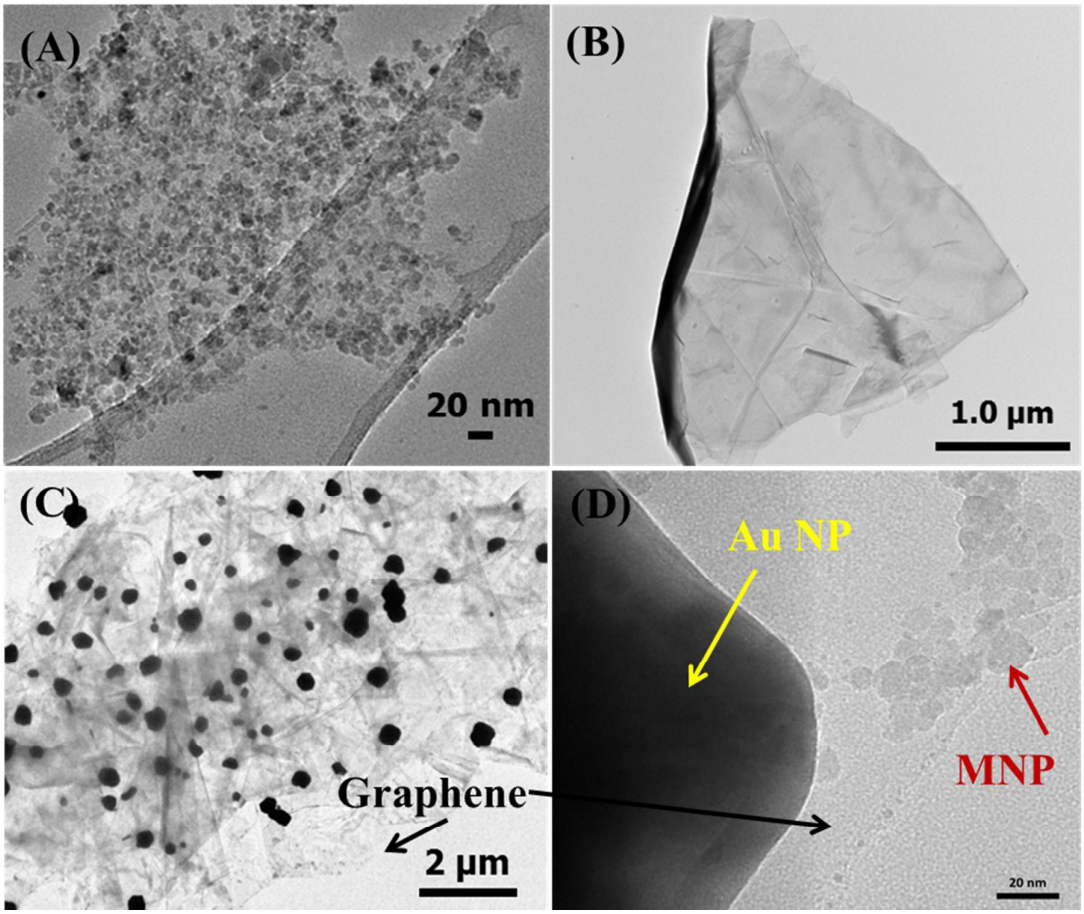

Figure 2. TEM images of (A) GA-MNP, (B) GRP, (C) Au/MNP-GRPs (low magnification, 4k ×) and (D) Au/MNP-GRPs (high magnification, 150k ×).

After preparation of the Au/MNP-GRPs, the morphologies and sizes of the nanomaterial were observed by TEM. GA-MNPs and GRP before the reaction are shown in Figures 2A and B, respectively. The size of GA-MNP is approximately 12 nm, and clear GRP sheets were observed. After 2 steps, two different types of particles appeared on the GRP sheets. The large black spots are Au NPs, whereas the small gray particles are MNPs. The Au NPs are non-spherical and widely dispersed on the surface of the GRP. The size of the Au NPs was approximately 200 nm, which is slightly larger than typical Au NPs because a surface capping agent was not applied for size control. Because the surface electron density of Au NPs is higher than that of MNPs, the Au NPs appear as black spots. Similar to Au NPs, GA-

MNPs are attached on the surface of GRP.

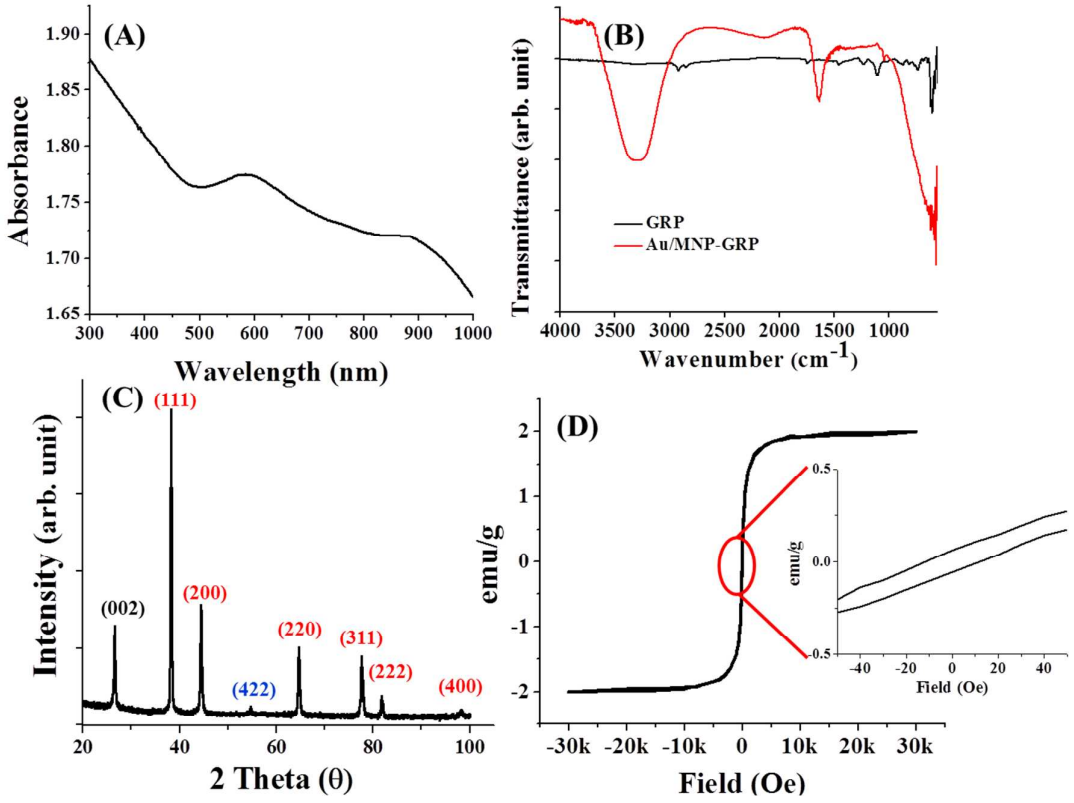

Figure 3. (A) UV/Vis and (B) FT-IR spectra, (C) XRD pattern (black; GRP, blue; GA-MNP, and red; Au NP) and (D) SQUID hysteresis curve of Au/MNP-GRPs

The physicochemical properties of the Au/MNP-GRPs are shown in Figure 3. The plasmonic property of the Au/MNP-GRPs was measured by UV/Vis spectroscopy. The absorbance of Au NPs is indicated at approximately 580 nm (Figure 3A), and this result is consistent with the size of the Au NPs in the TEM images.[30] As mentioned previously, the Au NPs are slightly larger in size; thus, λ_{max} is shown in that range. In addition, closely located Au NPs on the GRP sheet can induce the plasmonic coupling effect, which is observed at approximately 900 nm as the longitudinal direction coupling.[4,6] The functional groups of the Au/MNP-GRPs were analyzed by FT-IR spectroscopy. First, the Fe-O vibration from GA-MNP was approximately measured at 600 cm^{-1}. The aromatic ring in GRP was located at

approximately 1560-1455 cm^{-1}. The C=O vibration of GA appeared at approximately 1637 cm^{-1} (Figure 3B). Structural analysis of the Au/MNP-GRPs was conducted with XRD (Figure 3C). First, the diffraction pattern of GRP was indicated at 2 θ = 26.63° as the (002) plane (ICSD card no: 01−075−1621). In addition, several diffraction peaks of Au NPs, including the (111), (200), (220), (311), (222), and (400) planes, were identified at 2 θ = 38.37°, 44.67°, 64.62°, 77.49°, 81.69°, and 98.35°, respectively (ICSD card no: 00−004−0784). The (422) plane of iron oxide was measured at the 2 θ value of 54.44 (JCPDS card no: 88-0315). Magnetic property analysis of the Au/MNP-GRPs was performed using SQUID at room temperature from -30 kOe to 30 kOe. In this case, the magnetic-hysteresis relationship was expressed as a nonlinear and reversible hysteresis loop. According to the loop curve shown in Figure 3D, the coercive force of the Au/MNP-GRPs was approximately -20 Oe and 20 Oe. Indeed, the remanence effects were approximately 0.07 and -0.07 emu/g. Thus, GRP displays a magnetic property after the MNP decoration process.

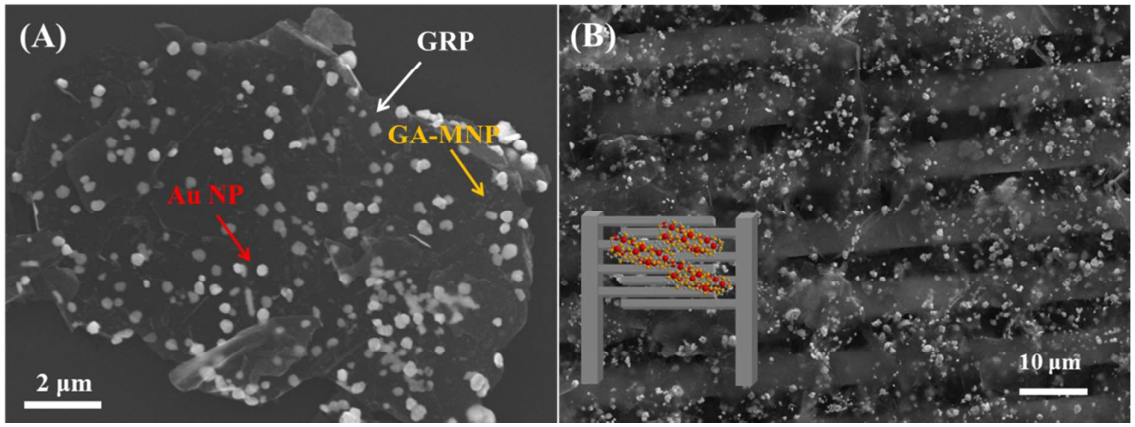

Figure 4. SEM images of (A) Au/MNP-GRPs on a Si wafer and (B) a Au/MNP-GRP sensing channel on Pt-IDE.

To magnetically deposit Au/MNP-GRPs onto the electrode, first, Pt-IDE was placed on the magnet (see Figure S1). In addition, to prevent spillage of solution from the electrode, a PDMS well was attached to the electrode. Au/MNP-GRP was gently dropped onto the electrode surface and dried under atmospheric conditions. The deposited Au/MNP-GRPs

were observed via SEM, and the image is shown in Figure 4. Au/MNP-GRPs on a Si wafer is shown in Figure 4A, and this image is consistent with the TEM image, where the Au NPs and GA-MNPs were dispersed on the GRP layer. In this case, the electrical density on the surface of GA-MNPs was lower than that of Au NPs, and the MNPs was much smaller than the Au NPs; thus, MNP structure was not clearly shown by SEM. Additionally, it was confirmed that the hybrid material was satisfactorily located on the Pt-IDE after magnetic deposition (Figure 4B). In this image, the Au/MNP-GRP layer was clearly observed and was well spread on the Pt-IDE. In addition, because the layer of Au/MNP-GRPs was thin, the Pt-IDE could be observed under the hybrid carbon nanomaterial.

The EDC/NHS coupling reaction between norovirus Ab and the amine group of Au/MNP-GRPs occurred on the Pt-IDE in the PDMS. Before the NoV-LP-sensing demonstration, an ELISA was performed to prove that the Ab had conjugated with the Au/MNP-GRPs (Figure S2). According to the ELISA result, the absorbance of Au/MNP-GRPs was higher than that of BSA. Thus, the norovirus Ab was successfully conjugated on the surface of the Au/MNP-GRPs. The conjugation reaction between the Ab and the Au/MNP-GRPs was performed on the Pt-IDE to detect NoV-LPs based on the resistance change. In this study, an external magnetic force was applied to deposit Au/MNP-GRPs with the aim of improving the sensing behavior and reduce contact resistance.[31] Using external magnetic force, stacking of the Au/MNP-GRPs occurred on the Pt-IDE, and this phenomenon reduced the contact resistance between Au/MNP-GRP structures. As a result, the sensing behavior could be improved to when compared Au/MNP-GRPs were deposited without magnetic force. In the case of magnetic deposition, the sensing performance was improved to a greater extent than that without the magnetic deposition process (Figure S3).

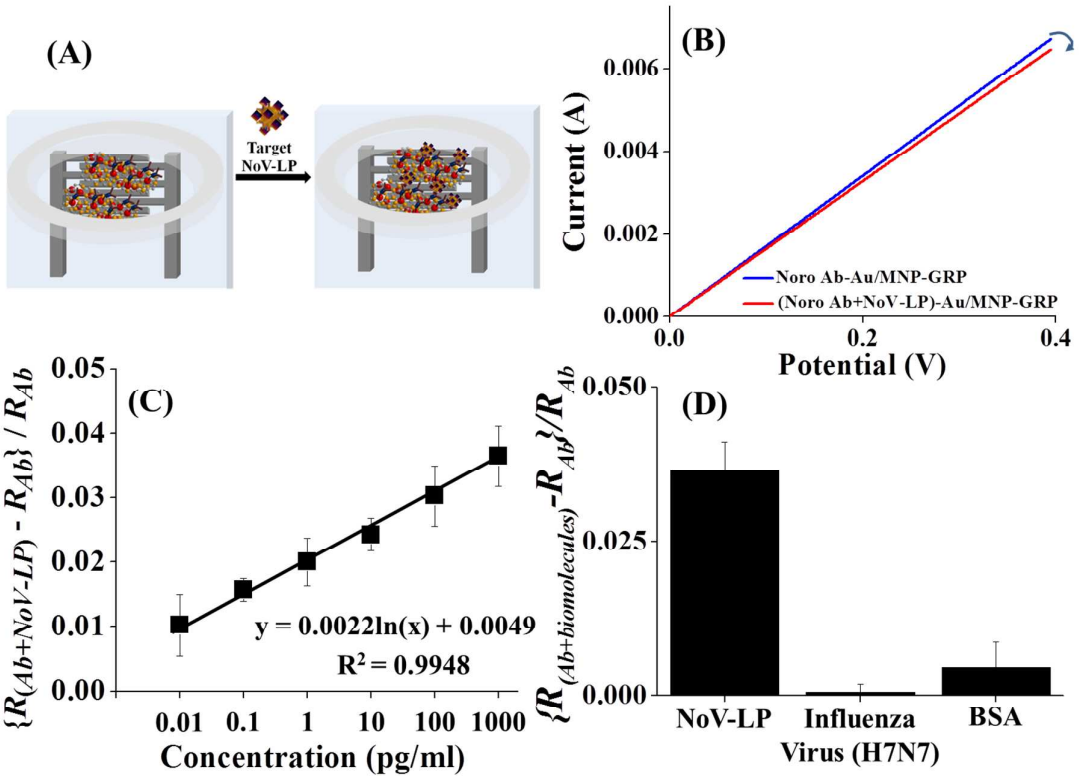

Figure 5. (A) Virus detection process with hybrid materials (not to scale), (B) IV curve for conductivity measurement of norovirus Ab-conjugated Au/MNP-GRPs (R_{Ab}) and NoV-LP-bound-norovirus Ab-conjugated Au/MNP-GRPs ($R_{(Ab+NoV-LP)}$) on the IDE; (C) NoV-LP concentration-dependent resistance difference ($\{R_{(Ab+NoV-LP)} - R_{Ab}\}/R_{Ab}$) for the sensitivity test, and (D) specificity test with the influenza antigen (H7N7) and BSA.

The detection mechanism of the target infectious pathogen is notably simple and is illustrated in Figure 5A. In brief, this system monitors the target biomolecules or biomaterials according to the change in electrical resistance. When the target biomolecules bind the Au/MNP-GRPs through biological affinity in this system, the resistance of the Au/MNP-GRPs increases. The electrical conductivity change after Ab modification on the Au/MNP-GRPs occurred and was also decreased (Figure S4). However, to monitor the Ab-NoV-LP conjugation for biosensing performance, in this case, it was considered that R_0 was R_{Ab}. The value of $\Delta R = \{R_{(\mathrm{Ab+vlp})} - R_{\mathrm{Ab}}\}$ depends on the concentration of target biomolecules. Based on this type of approach, the sensing behavior of the Au/MNP-GRP-deposited Pt-IDE

was demonstrated using various concentrations of NoV-LPs (Figure 5). When the target NoV-LPs were added (Figure 5A), the conductivity of the Ab-conjugated Au/MNP-GRPs (blue line) decreased after the NoV-LPs bound Ab-conjugated Au/MNP-GRPs (red line) in this sensing system (Figure 5B). Thus, the concept of this system was demonstrated by monitoring the conductivity change. Subsequently, the detection sensitivity of the Au/MNP-GRP-based sensing system was characterized with NoV-LP concentrations ranging from 0.01 pg/ml to 1 ng/ml. As expected, the conductivity decreased with an increase in NoV-LP concentration. To verify the sensitivity, the resistance at each concentration was normalized ($\triangle R/R_{Ab}$) and compared (Figure 5C). According to Equation S1 in the SI, the limit of detection (LOD) of this system was calculated as 1.16 pg/ml; thus, this sytstem shows excellent sensitivity. It is well known that the sensitivity of the commercial diagnostic kit for norovirus is approximately 1 ng/ml. Thus, the norovirus sensitivity of this sensing platform offers dramatically improved performance (by a factor of approximately 10^3). However, the sensing behavior was also related to the amount of sensing channels, which means that the sensitivity could change depending on the amount of Au/MNP-GRPs. When a smaller amount of Au/MNP-GRPs (20 μg) was deposited on the Pt-IDE, the results of the sensitivity test (Figure S5) still exhibited a linear calibration curve, but the standard deviation was too wide; this low reliability is acknowledged. The specificity test of this system was performed using the influenza virus antigen and BSA. As shown in Figure 5D, a high response ($\triangle R$) was only obtained in the NoV-LP case, whereas the resistance change was not clearly observed in the other cases, which indicates that this system has high specificity. Thus, our system shows high potential for use in biosensing systems.

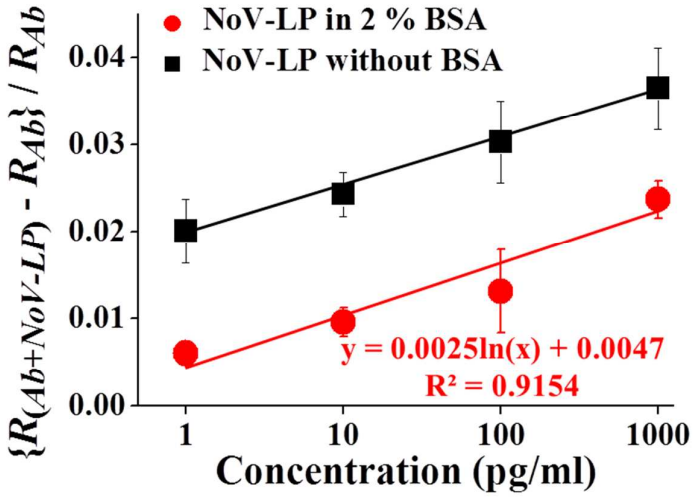

Figure 6. Sensing behavior test depending on the background impact by using NoV-LP mixed with (●) /without (■) 2 % BSA

On the other hands, it would be considered that target biomolecule could be existed with other matrix in the real situation and field. Thus, in order to evaluate the sensing behavior of this system against background impact, various concentration from 1 pg/ml to 1000 pg/ml of NoV-LP were mixed in 2 % BSA solution as a biological complex medium and these mixtures have been monitored by Au/MNP-GRP based sensing channel. In this case, though large amount of proteins was mixed NoV-LP, the target NoV-LP could be detected as shown in Figure 6. The density of proteins in the mixture is much higher than that of NoV-LP and sample was not homogenous environment, so, binding hindrance between target VLP and Ab could be occurred by high dense background impact. And as a result, low $\triangle R/R_{Ab}$ was obtained in complex medium. This is the reason that a correlation coefficient, R^2 value and sensitivity in NoV-LP/BSA mixture (red circle) was lower than that value in NoV-LP/buffer (black square). However, the potential was shown that against of background impact which contains high amount of BSA, low concentrations of NoV-LP were successfully detected by Au/MNP-GRP sensing channel.

4. CONCLUSIONS

In our study, Au/MNP-GRPs were successfully prepared in two simple steps, and both particles were well dispersed on the GRP surface. This hybrid structure has excellent electrical conductivity and a magnetic property. Thus, based on these multi-functionalities, the Au/MNP-GRPs can play a role in bio-sensing channels. To demonstrate the biosensing application, Au/MNP-GRPs were deposited on a Pt-IDE via an external magnetic force, and the surface of this hybrid material was conjugated with the GII type of norovirus-specific Ab. In this case, the resistance difference of Ab-Au/MNP-GRPs was monitored based on the concentration of NoV-LPs. The system showed an excellent sensitivity level, and the LOD was calculated as 1.16 pg/ml. In addition, the Au/MNP-GRP-based NoV-LP detection system exhibited good selectivity over that of other biomolecules such as influenza virus and BSA. In addition, NoV-LP was successfully monitored against high background impact. Thus, this hybrid nanomaterial has great potential for nanobiosensing applications.

■ ASSOCIATED CONTENT

Ⓢ Supporting information

Preparation of NoV-LPs, Calculation of detection limitation, Photo image of magnetically deposited Au/MNP-GRP sensing channel on Pt-IDE, ELISA result for norovirus Ab conjugation on Au/MNP-GRPs, Sensing performance of Au/MNP-GRP-sensing platform depending on the magnetic deposition process, IV curve change of Au/MNP-GRPs, Sensitivity test of NoV-LP using a lower amount (20 μg) of Au/MNP-GRPs deposited on the sensing channel.

■ AUTHOR INFORMATION

Corresponding author

*E-mail: park.enoch@shizuoka.ac.jp; Tel. & Fax: +81 54 238-4887

ORCID

Enoch Y. Park: 0000-0002-7840-1424

Notes

The authors declare no competing financial interest.

■ ACKNOWLEDGMENTS

This research was supported by the Japan Society for the Promotion of Science (JSPS) Postdoctoral Fellowship for Overseas Researchers (16F16361).

■ REFERENCES

(1) Lee, J.; Lee, K.; Park, S. Environmentally Friendly Preparation of Nanoparticle-Decorated Carbon Nanotube or Graphene Hybrid Structures and Their Potential Applications. *J. Mater. Sci.* **2016,** *51*, 2761–2770.

(2) Klinkova, A.; Choueiri, R. M.; Kumacheva, E. Self-Assembled Plasmonic Nanostructures. *Chem. Soc. Rev.* **2014,** *43*, 3976–3991.

(3) Lee, J.; Lee, J. Magneto-Optically Active Magnetoplasmonic Graphene. *Chem. Commun.* **2017,** *53*, 5814-5817.

(4) Lee, J.; Kim, J.; Ahmed, S. R.; Zhou, H.; Kim, J. M.; Lee, J. Plasmon-Induced Photoluminescence Immunoassay for Tuberculosis Monitoring Using Gold-Nanoparticle-Decorated Graphene. *ACS Appl. Mater. Interfaces* **2014,** *6*, 21380–21388.

(5) Lee, J.; Mulmi, S.; Thangadurai, V.; Park, S. S. Magnetically Aligned Iron Oxide/Gold Nanoparticles Decorated Carbon Nanotube Hybrid Structure as Humidity Sensor. *ACS Appl. Mater. Interfaces* **2015,** *7*, 15506–15513.

(6) Lee, J.; Ahmed, S. R.; Oh, S.; Kim, J.; Suzuki, T.; Parmar, K.; Park, S. S.; Lee, J.; Park, E. Y. A Plasmon-Assisted Fluoro-Immunoassay Using Gold Nanoparticle-Decorated Carbon Nanotubes for Monitoring the Influenza Virus. *Biosens. Bioelectron.* **2015,** *64*, 311–317.

(7) Ahmed, S. R.; Kim, J.; Suzuki, T.; Lee, J.; Park, E. Y. Enhanced Catalytic Activity of Gold Nanoparticle-Carbon Nanotube Hybrids for Influenza Virus Detection. *Biosens. Bioelectron.* **2016,** *85*, 503–508.

(8) Zanolli, Z.; Leghrib, R.; Felten, A.; Pireaux, J. J.; Llobet, E.; Charlier, J. C. Gas

Sensing with Au-Decorated Carbon Nanotubes. *ACS Nano* **2011,** *5*, 4592–4599.

(9) Kim, J.; Jang, M.; Lee, K. G.; Lee, K. S.; Lee, S. J.; Ro, K. W.; Kang, I. S.; Je ong, B. D.; Park, T. J.; Kim, H. J. Plastic-Chip-Based Magnetophoretic Immunoassay for Point-of-Care Diagnosis of Tuberculosis. *ACS Appl. Mater. Interfaces* **2016,** *8*, 234 89–23497.

(10) Ahmed, S. R.; Takemeura, K.; Li, T. C.; Kitamoto, N.; Tanaka, T.; Suzuki, T.; Park, E. Y. Size-Controlled Preparation of Peroxidase-Like Graphene-Gold Nanoparticl e Hybrids for the Visible Detection of Norovirus-Like Particles. *Biosens. Bioelectron.* **2017,** *87*, 558–565.

(11) Ahmed, S. R.; Kim, J.; Tran, V. T.; Suzuki, T.; Neethirajan, S.; Lee, J.; Park, E. Y. In Situ Self-Assembly of Gold Nanoparticles on Hydrophilic and Hydrophobic Su bstrates for Influenza Virus-Sensing Platform. *Sci. Rep.* **2017,** *7*, 44495.

(12) Kim, J.; Lee, K. S.; Kim, E. B.; Paik, S.; Chang, C. L.; Park, T. J.; Kim, H. J.; Lee, J. Early Detection of the Growth of Mycobacterium Tuberculosis Using Magn etophoretic Immunoassay in Liquid Culture. *Biosens. Bioelectron.* **2017,** *96*, 68–76.

(13) Al-Tawfiq, J. A.; Zumla, A.; Gautret, P.; Gray, G. C.; Hui, D. S.; Al-Rabeeah, A. A.; Memish, Z. A. Surveillance for Emerging Respiratory Viruses. *Lancet Infect. D is.* **2014,** *14*, 992–1000.

(14) Deng, X.; Chen, M.; Fu, Q.; Smeets, N. M. B.; Xu, F.; Zhang, Z.; Filipe, C. D. M.; Hoare, T. A Highly Sensitive Immunosorbent Assay Based on Biotinylated Grap hene Oxide and the Quartz Crystal Microbalance. *ACS Appl. Mater. Interfaces* **2016,** *8*, 1893–1902.

(15) Duan, B.; Zhou, J.; Fang, Z.; Wang, C.; Wang, X.; Hemond, H. F.; Chan-Park, M. B.; Duan, H. Surface Enhanced Raman Scattering by Graphene-Nanosheet-Gapped Plasmonic Nanoparticle Arrays for Multiplexed DNA Detection. *Nanoscale* **2015,** *7*, 12 60612613.

(16) Elshafey, R.; Siaj, M.; Tavares, A. C. Au Nanoparticle Decorated Graphene Nano Sheets for Electrochemical Immunosensing of p53 Antibodies for Cancer Prognosis. *A nalyst* **2016,** *141*, 2733–2740.

(17) Gao, Z.; Kang, H.; Naylor, C. H.; Streller, F.; Ducos, P.; Serrano, M. D.; Ping, J.; Zauberman, J.; Rajesh; Carpick, R. W.; Wang, Y. J.; Park, Y. W.; Luo, Z.; Ren, L.; Johnson, A. T. C. Scalable Production of Sensor Arrays Based on High-Mobility Hybrid Graphene Field Effect Transistors. *ACS Appl. Mater. Interfaces* **2016,** *8*, 27546 –27552.

(18) Kwan, H. S.; Chan, P. K. S.; Chan, M. C. W. Chapter 2 - Overview of Norovir us as a Foodborne Pathogen. *In The Norovirus*, 2017; pp 21–30.

(19) Scallan, E.; Hoekstra, R. M.; Angulo, F. J.; Tauxe, R. V.; Widdowson, M. A.; R oy, S. L.; Jones, J. L.; Griffin, P. M. Foodborne Illness Acquired in the United States -Major Pathogens. *Emerg. Infect. Dis.* **2011,** *17*, 7–15.

(20) Batz, M. B.; Hoffmann, S.; Morris Jr, J. G. Ranking the Disease Burden of 14 Pathogens in Food Sources in the United States Using Attribution Data From Outbrea k Investigations and Expert Elicitation. *J. Food Prot.* **2012,** *75*, 1278–1291.

(21) Koho, T.; Ihalainen, T. O.; Stark, M.; Uusi-Kerttula, H.; Wieneke, R.; Rahikainen, R.; Blazevic, V.; Marjomäki, V.; Tampé R.; Kulomaa, M. S.; Hytönen, V. P. His-Tad gged Norovirus-Like Particles: A Versatile Platform for Cellular Delivery and Surface Display. *Eur. J. Pharm. Biopharm.* **2015**, *96,* 22–31.

(22) Ushihima, H.; Thongprachum, A.; Okitsu, S.; Khamrin, P. Chapter 11-Immunochr omatographic Tests for Rapid Diagnosis of Noroviruses. *In The Norovirus ,* 2017; pp 155–162.

(23) Fraisse, A.; Coudray-Meunier, C.; Martin-Latil, S.; Hennechart-Collette, C.; Delan noy, S.; Fach, P.; Perelle, S. Digital RT-PCR Method for Hepatitis A Virus and Noro virus Quantification in Soft Berries. *Int. J. Food Microbiol.* **2017,** *243,* 36–45.

(24) Ramanan, P.; Espy, M. J.; Khare, R.; Binnicker, M. J. Detection and Differentiati on of Norovirus Genogroups I and II from Clinical Stool Specimens using Real-Time PCR. *Diagn. Microbiol. Infect. Dis.* **2017,** *87*, 325–327.

(25) Karst, S. M.; Wobus, C. E.; Goodfellow, I. G.; Green, K. Y.; Virgin, H. W. Adv ances in Norovirus Biology. *Cell Host Microbe* **2014,** *15*, 668–680.

(26) Orchard, R. C.; Wilen, C. B.; Doench, J. G.; Baldridge, M. T.; McCune, B. T.; Lee, Y. C.; Lee, S.; Pruett-Miller, S. M.; Nelson, C. A.; Fremont, D. H. Discovery of a Proteinaceous Cellular Receptor for a Norovirus. *Science* **2016,** *353*, 933–936.

(27) Takemura, K.; Adegoke, O.; Takahashi, N.; Kato, T.; Li, T. C.; Kitamoto, N.; Ta naka, T.; Suzuki, T.; Park, E. Y. Versatility of a Localized Surface Plasmon Resonanc e-Based Gold Nanoparticle-Alloyed Quantum Dot Nanobiosensor for Immunofluorescen ce Detection of Viruses. *Biosens. Bioelectron.* **2017,** *89,* 998–1005.

(28) Kitamoto, N.; Tanaka, T.; Natori, K.; Takeda, N.; Nakata, S.; Jiang, X.; Estes, M. K. Cross-Reactivity Among Several Recombinant Calicivirus Virus-like Particles (VLP s) with Monoclonal Antibodies Obtained from Mice Immunized Orally with One Type of VLP. *J. Clin. Microbiol.* **2002**, *40*, 2459-2465.

(29) Lee, J.; Kim, H. Y.; Zhou, H.; Hwang, S.; Koh, K.; Han, D. W.; Lee, J. Green Synthesis of Phytochemical-Stabilized Au Nanoparticles under Ambient Conditions and Their Biocompatibility and Antioxidative Activity. *J. Mater. Chem.* **2011,** *21*, 13316–13326.

(30) Lee, J.; Zhou, H.; Lee, J. Small Molecule Induced Self-Assembly of Au Nanopar ticles. *J. Mater. Chem.* **2011,** *21*, 16935–16942.

(31) Tran, V. T; Zhou, H.; Kim, S.; Lee, J.; Kim, J.; Zou, F.; Kim, J. Park, J. Y.; Lee, J. Self-Assembled Magnetoplasmonic Nanochain for DNA Sensing, *Sens. Actuator B-Chem.*, **2014**, *203*, 817-823.

Antibody (Ab)
Au NP
GA-MNP
Graphene sheet
(I) Au^{3+}
(II) GA-MNP
NoV-LP
Noro Ab-Au/MNP-GRP
(Noro Ab+NoV-LP)-Au/MNP-GRP
Current (A)
Potential (V)